Electric-field-induced and spontaneous relaxor-ferroelectric phase transitions in $(Na_{1/2}Bi_{1/2})_{1-x}Ba_xTiO_3$

Cite as: J. Appl. Phys. **112**, 124106 (2012); https://doi.org/10.1063/1.4770326
Submitted: 20 October 2012 • Accepted: 19 November 2012 • Published Online: 20 December 2012

F. Craciun, C. Galassi and R. Birjega

Electric-field-induced and spontaneous relaxor-ferroelectric phase transitions in $(Na_{1/2}Bi_{1/2})_{1-x}Ba_xTiO_3$

F. Craciun,[1,a] C. Galassi,[2] and R. Birjega[3]
[1]*CNR-ISC, Istituto dei Sistemi Complessi, Area della Ricerca di Roma-Tor Vergata, Via del Fosso del Cavaliere 100, I-00133 Roma, Italy*
[2]*CNR-ISTEC, Istituto di Scienza e Tecnologia dei Materiali Ceramici, Via Granarolo 64, I-48018 Faenza, Italy*
[3]*NILPRP, P.O. Box MG-16, RO-77125 Bucharest, Romania*

(Received 20 October 2012; accepted 19 November 2012; published online 20 December 2012)

Complex dielectric susceptibility was used to investigate the relaxor properties and the ferroelectric phase transitions in $(Na_{1/2}Bi_{1/2})_{1-x}Ba_xTiO_3$ ($0 \le x \le 0.08$) ceramics. XRD was used to characterize the ground states of poled and unpoled samples. Dielectric susceptibility vs. temperature studies allowed to obtain the relaxor properties and to identify the electric field-induced phase transitions in the morphotropic phase boundary (MPB) compositions ($0.06 < x < 0.08$) and the spontaneous relaxor-ferroelectric phase transitions in the rhombohedral compositions ($x < 0.06$). The frequency dispersion of the dielectric maximum at T_m was observed for all compositions, although of decreased extension for lower x. The relaxor properties have been analysed with Vogel-Fulcher law. The activation energy and attempt frequency for the MPB compositions are similar to those of classical relaxors like $Pb(Mg_{1/3}Nb_{2/3})O_3$, while for rhombohedral compositions, they are similar to relaxor ferroelectrics with spontaneous relaxor-ferroelectric phase transitions, like $Pb(Sc_{1/2}Nb_{1/2})O_3$. A relationship has been found between the relaxor dispersion degree and the hysteresis of the ferroelectric transition. © *2012 American Institute of Physics*. [http://dx.doi.org/10.1063/1.4770326]

I. INTRODUCTION

Extensive studies of $(Na_{1/2}Bi_{1/2})_{1-x}Ba_xTiO_3$ (NBT-BT) piezoelectrics have demonstrated their potential as substitute for lead zirconate titanate materials[1–4] and clarified many uncertain points in their phase diagram.[1,5–11] Detailed structural investigations by neutron diffraction[12] evidenced the polymorphic structure of $(Na_{1/2}Bi_{1/2})TiO_3$ (NBT) that, above 810 K, belongs to the cubic symmetry (space group $Pm\bar{3}m$), while below 810 K and down to about 600 K, a tetragonal P4bm phase is established and further transforms into the rhombohedral R3c ground state; the boundaries between these states are not sharp, and broad regions of phase coexistence have been found.[12]

A systematic x-ray diffraction study (XRD)[13] of the evolution of crystallographic phases with x evidenced significant differences between the unit cell parameters of poled and unpoled samples. A morphotropic phase boundary (MPB) at $0.06 \le x \le 0.08$, previously identified by different techniques,[1,4,5] has been confirmed.

The evolution of the domain structures with x has been investigated with piezoresponse force microscopy (PFM) and transmission electron microscopy (TEM).[14,15] It has been found that, with increasing of x, the size of polar nanoregions (PNRs), already present in NBT,[16] is refined and their self-organization is enhanced. Domain morphology and crystal structure have been investigated with TEM[7] for compositions $x = 0.04$–0.11, below and around MPB. Thus, it was found that below 0.06, the ground state of unpoled samples has rhombohedral R3c symmetry with ferroelectric domains of about 100 nm, while only nanodomains with tetragonal P4bm symmetry have been evidenced in the compositions $0.07 \le x \le 0.09$. Above MPB, samples with $x = 0.11$ displayed large lamellar ferroelectric domains with tetragonal P4mm symmetry. Hot stage TEM[17] on $x = 0.06$ and $x = 0.11$ samples evidenced that both ferroelectric R3c and P4mm domains transform, above a temperature called depolarization temperature (T_d), in ferrielectric P4bm nanodomains, which further gradually evolve into $Pm\bar{3}m$ cubic structure.

The MPB itself is rather elusive, is placed at different x values by different authors, and very recent studies[10] have established its strong dependence on the electrical poling.

Dielectric investigations[1–9,18–20] evidenced a ferroelectric phase transition at T_d and a broad maximum at T_m, not related to any structural transformation. Both T_m and T_d vary with x and with the polarization state of the samples. The value of the dielectric constant is maximum for x in the MPB range.[1–5]

Previous anelastic measurements[8] on samples with $0 \le x \le 0.8$ evidenced an elastic anomaly associated with rhombohedral-tetragonal phase transition. This is extremely sharp in NBT and occurs at a temperature T_2 much higher than the ferroelectric transition T_d. T_2 decreases rapidly and merges with T_d at $x = 0.02$–0.03, to become again separated above $x = 0.06$. A sharp elastic anomaly signals also the cubic-tetragonal transition temperature T_1 in NBT. T_1 drops rapidly with x toward T_m, and the associated elastic anomaly becomes very broadened for $x > 0.05$. This broad anomaly is due to the large structural phase region where the tetragonal-to-cubic-phase transition develops progressively, with the

[a]Author to whom correspondence should be addressed. Electronic mail: Floriana.Craciun@isc.cnr.it. Tel. +39 0649934024. Fax: +39 0645488003.

size and population of P4bm nanodomains decreasing with increasing temperature, as evidenced by hot-stage TEM.[17]

In the light of these previous findings, we analyze our results obtained from x-ray diffraction and complex dielectric permittivity measurements on poled and unpoled samples with $0 \leq x \leq 0.8$, especially the dispersion at T_m and the extension of ferroelectric phase on heating and cooling.

II. EXPERIMENT

The ceramic samples of the composition $(Na_{1/2}Bi_{1/2})_{1-x}Ba_xTiO_3$ with $x = 0.0$, 0.02, 0.03, 0.04, 0.05, 0.06, 0.065, 0.07, 0.075, and 0.08 have been prepared by a solid state reaction synthesis, as previously described.[8] Stoichiometric amounts of the starting oxides/carbonates were milled and mixed in ethanol, dried, and sieved. After heat treatment at 700–800 °C for 1 h, the powders have been isostatically pressed and sintered at 1150 °C for 2 h, in alumina crucibles sealed with NBT pack, to avoid losses. The densities were about 98% of the theoretical ones.

The crystalline structure of the samples was examined with a PANalytical X'pert MRD diffractometer in conventional Bragg-Brentano geometry using the filtered CuK_α ($\lambda = 0.154$ nm) radiation in a continuous mode. Each sample was scanned through a 2θ range of 20°–100° with a step size of 0.02° and with a scanning time on step of 25 s or 250 s, depending on the angular range.

The XRD spectra were analyzed with the PANALYTICAL X'PERT HIGH SCORE PLUS software package. The crystalline phases were identified using the data base provided by the JCPDS-International Centre for Diffraction Data (ICDD). Measurements have been performed both on poled and unpoled samples.

The samples for dielectric measurements were silver electroded and poled under an electric field of 3 kV/mm in a silicon oil bath at 120 °C for 30 min.

The dielectric measurements were carried out on poled and unpoled samples in the frequency range 200 Hz-1 MHz with an HP 4284A LCR bridge, by using a four wire probe and an ac driving signal level of 0.5 V/mm. The dielectric permittivity $\varepsilon = \varepsilon' - i\varepsilon''$ was obtained from the measured values of capacitance and loss $\tan\delta = \varepsilon''/\varepsilon'$. The measurements were made on heating and cooling at 1–1.5 K/min between 300 and 570 K in a Delta Design climatic chamber (model 9023A).

III. RESULTS AND DISCUSSION

A. Structural properties

Fig. 1 shows XRD spectra taken on unpoled samples with different compositions ($0 \leq x \leq 0.8$) while Fig. 2 shows the results obtained on poled samples. As mentioned above, the poled state is that achieved under a dc field of 3 kV/mm, for all the compositions. It can be observed that the effect of poling on rhombohedral (R)($x = 0 \div 0.05$) and tetragonal (T) ($x = 0.08$) compositions is to increase the corresponding R and T splittings, respectively. However, the most dramatic difference is registered for the MPB compositions (represented in the graph by $x = 0.06$), which, unpoled, shows a

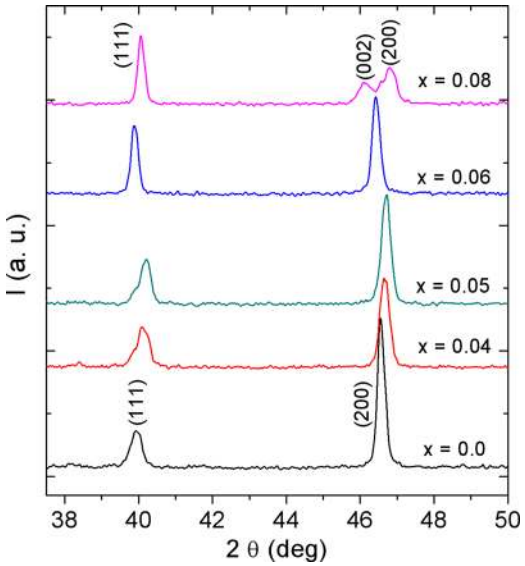

FIG. 1. Details from XRD spectra showing evolution of (111) and (200) reflection peaks with composition in unpoled NBT-BT samples.

cubic structure, while poled shows splitting of the cubic (111) reflection into (111) and (−111) peaks of the rhombohedral (pseudocubic) phase and the splitting of the cubic (200) reflection into (002) and (200) peaks of the tetragonal phase. The observation of both R and T splittings indicate coexistence of R and T phases (MPB) after poling. A shoulder can be observed also near the (200) peak of poled $x = 0.05$ composition (Fig. 2), indicating the appearance of a tetragonal phase after poling.

The weak peak at $2\theta \approx 38.2°$ in Fig. 2 represents the superlattice peak 1/2(311) indexed with respect to the pseudocubic cell. It is visible only in the reflection spectra corresponding to poled samples. This superlattice reflection corresponds, in Glazer's notation,[21] to $a^-a^-a^-$ tilt system (space group R3c). Its evolution with x can be followed better in Fig. 3, where it can be observed up to $x = 0.06$ composition.

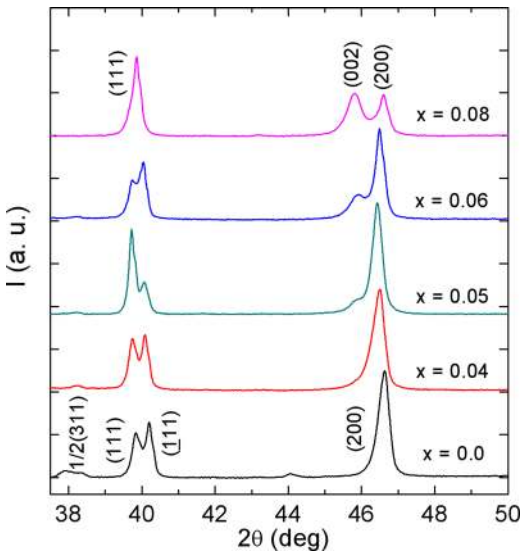

FIG. 2. The same as in Fig. 1 but for poled NBT-BT samples.

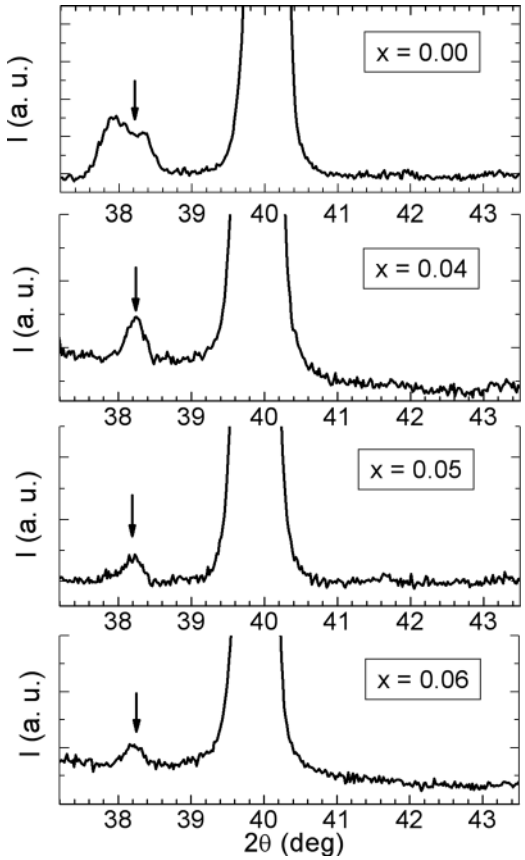

FIG. 3. Details from XRD spectra of poled NBT-BT samples showing evolution of ½ (311) superlattice reflection (marked by arrows) with x.

One must note that both 0.04 and 0.05 compositions show R splitting on unpoled samples, as can be observed in Fig. 4, where the fitting of the (111)/(−111) reflections for 0.05 composition is shown, and this splitting is further increased by poling (Fig. 2).

Details corresponding to (111) (Fig. 5(a)) and (200) (Fig. 5(b)) reflection peaks from the XRD spectra of poled and unpoled samples with x = 0.06 evidence better the transformation of the cubic structure into R + T phase coexistence (MPB) following the poling treatment.

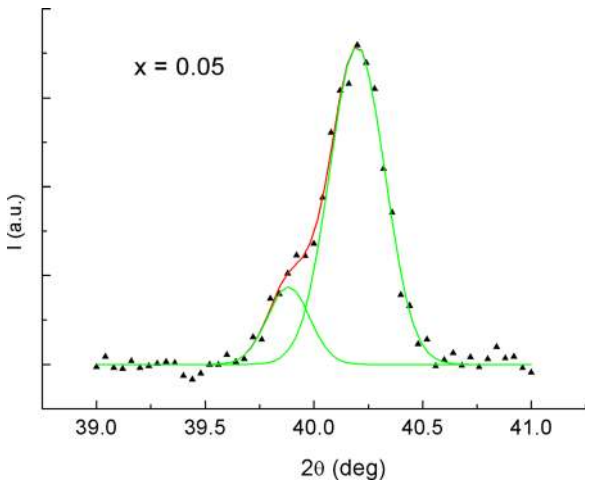

FIG. 4. (111)/(−111) peak splitting in unpoled x = 0.05 sample.

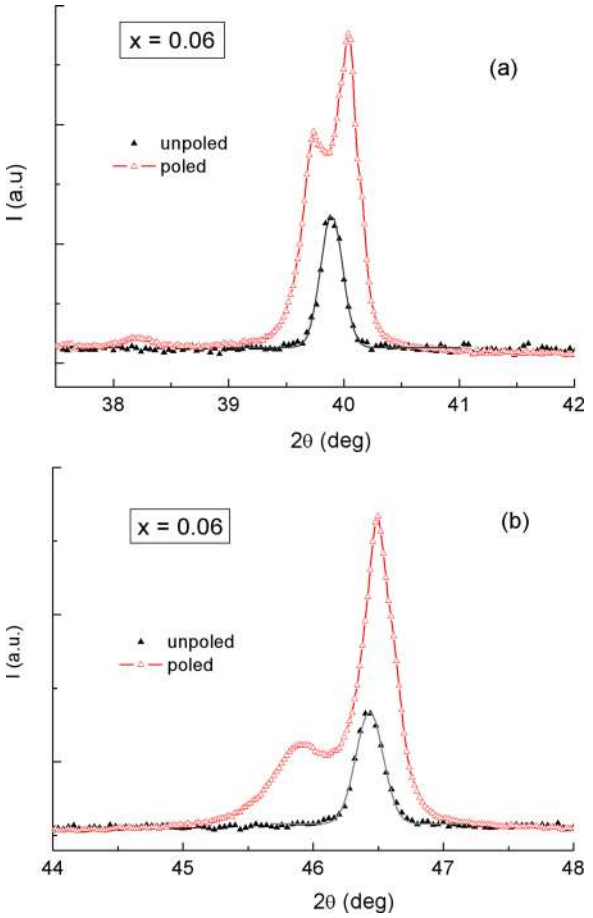

FIG. 5. (a) (111)/(−111) peak splitting in poled x = 0.06 sample compared with the (111) peak in the unpoled sample; (b) (002)/200) peak splitting in poled x = 0.06 sample compared with the (200) peak in the unpoled sample.

In Fig. 6, the values of the tetragonal $\Delta\theta_{tr}$ (upper graph) and rhombohedral $\Delta\theta_{rh}$ (lower graph) splittings derived from the (200) and (111) peaks splittings, on poled (empty symbols) and unpoled (full symbols) samples have been plotted as a function of x. Star symbols represent results on two R (x = 0.03) and T (x = 0.07) compositions taken from Ref. 13. It can be observed that the highest increasing of splittings of poled samples with respect to unpoled is obtained for x in the MPB region. An important increase of the rhombohedral $\Delta\theta_{rh}$ splitting is obtained also for NBT, while smaller variations are registered for compositions in the range 0.03 ÷ 0.05.

B. Dielectric spectra

1. MPB compositions

Fig. 7 shows real ε' and imaginary ε'' permittivities versus temperature, measured on an unpoled 0.06 sample at five frequencies in the range 200 Hz–1 MHz, both on heating and cooling. No thermal hysteresis between heating and cooling curves can be observed. On the graph, T_m marks the temperature of the dielectric permittivity maximum, which shifts with frequency ω increasing towards higher temperatures, a behavior typical for relaxor ferroelectrics.[22,23] Indeed, a key feature of relaxors is the appearance of a broad temperature and frequency dependent maximum of the dielectric

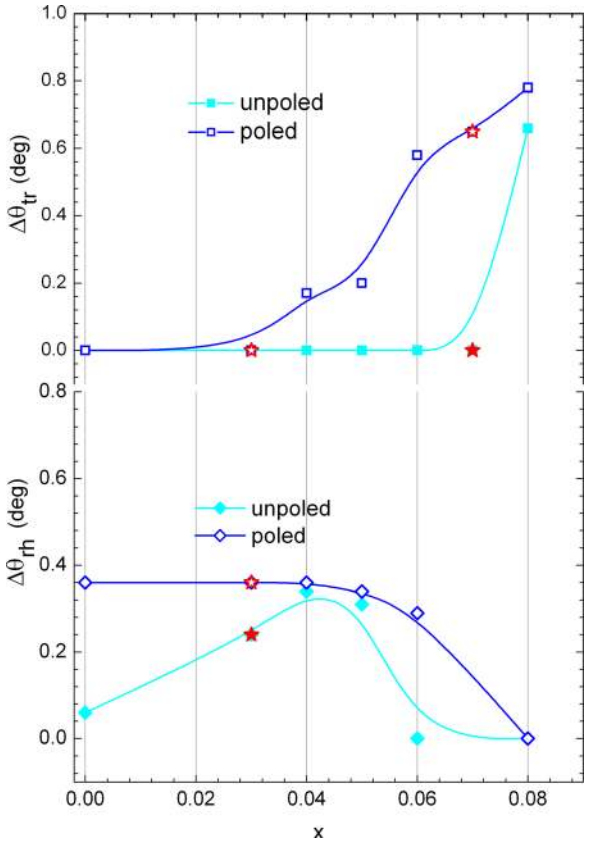

FIG. 6. Tetragonal $\Delta\theta_{tr}$ (upper graph) and rhombohedral $\Delta\theta_{rh}$ (lower graph) splittings obtained from the (200) and (111) peaks splittings, on poled (empty symbols) and unpoled (full symbols) samples as a function of x. Star symbols represent results on two R (x = 0.03) and T (x = 0.07) compositions taken from Ref. 13.

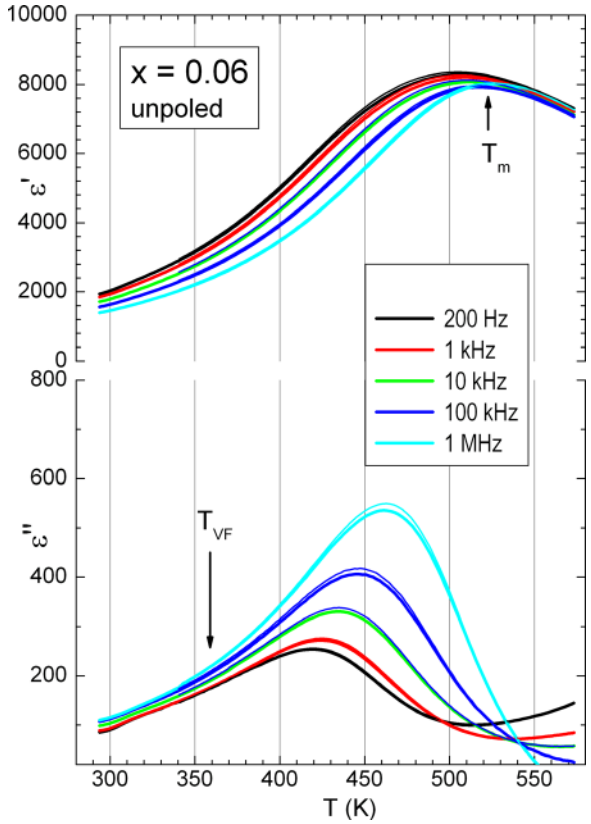

FIG. 7. Real ε' and imaginary ε'' permittivities versus temperature, measured on an unpoled x = 0.06 sample at five frequencies in the range 200 Hz–1 MHz, both on heating and cooling.

permittivity ε (ω,T) as well as the absence of long-range ferroelectric order in zero field at any temperature.[22,23] On the graphs, T_{VF} is the Vogel-Fulcher (VF) temperature[22,23] that will be further discussed. No other anomaly excepting the broad peak at T_m has been found.

Dielectric measurements on x = 0.06 poled samples are shown in Fig. 8. The heating curves display mainly a ferroelectric transition from a ferroelectric phase at low temperature to a relaxor phase at the temperature marked by T_d, identified by a kink. Temperature T_2 has been identified by anelastic measurements[8] as the temperature of transition from R to T phase.

Similar dielectric behavior is shown also by other samples in the MPB region.

Dielectric measurements on x = 0.08 samples show also differences between unpoled (Fig. 9) and poled (Fig. 10) samples. The kink in the ε' and ε'' curves for poled samples (Fig. 10) indicates the transition from ferroelectric to relaxor phase. Although tetragonal as structure, the dielectric behavior of this sample is similar to MPB compositions, therefore we preferred to discuss its behavior in this context. We return latter to this point.

The relaxor behavior found in MPB compositions is obviously due to the existence of polar nanoregions, directly evidenced by TEM.[7,24] This picture corresponds also to Ref. 24, where bright field TEM image of a x = 0.06 unpoled sample at room temperature revealed only a grainy contrast and no trace of ferroelectric domains, while selected area electron diffraction (SAED) on the same region revealed that each grain had a trace of R3c and tetragonal P4bm symmetry, indicated by the presence of $^1/_2$(ooo) and $^1/_2$(ooe) (o = odd and e = even) superlattice reflections. These regions must have nanoscale dimension, since no splitting in XRD reflections was detected, like in our Fig. 1 (curve corresponding to x = 0.06 sample). TEM bright field images reported in Ref. 7 shown that the ground state of MPB samples x = 0.07 and x = 0.09 was formed only by nanodomains. Moreover, SAED patterns on the same area exhibited $^1/_2$ (ooe) spots along the [111] zone axis, characteristic of the P4bm symmetry with $a^0a^0c^+$ oxygen octahedron tilt. Our unpoled x = 0.06 sample could have a similar ground state, formed only of nanodomains, since its XRD patterns reveals a pseudocubic structure with no significant distortions (Fig. 1).

Moreover, according to Ref. 7, our unpoled x = 0.08 sample should have a ground state formed of P4bm nanodomains. This would be in agreement with the relaxor behavior displayed in Fig. 9, but in contradiction with XRD spectra, which shows that the system has already a tetragonal splitting in the unpoled state (Fig. 1). We presume that the ground state of this system could be a mix of P4bm nanodomains and P4mm lamellar domains, somehow like in x = 0.11 samples investigated in Ref. 7, but with smaller concentration of P4mm phase. The tetragonal P4mm phase could be in sufficient amount to be revealed in XRD spectra by the splitting of (200) peak (one must note however the

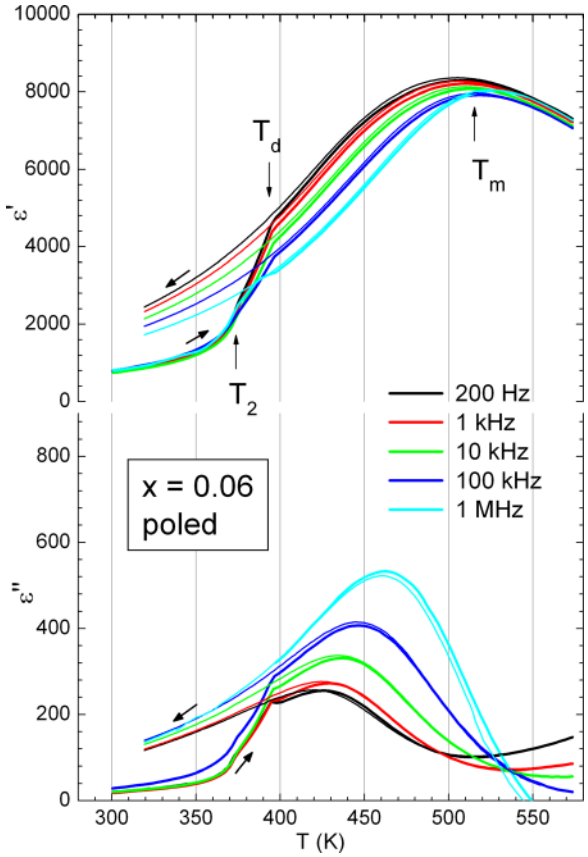

FIG. 8. The same as in Fig. 7, but on a poled x = 0.06 sample. The short arrows near the curves mark the heating and cooling.

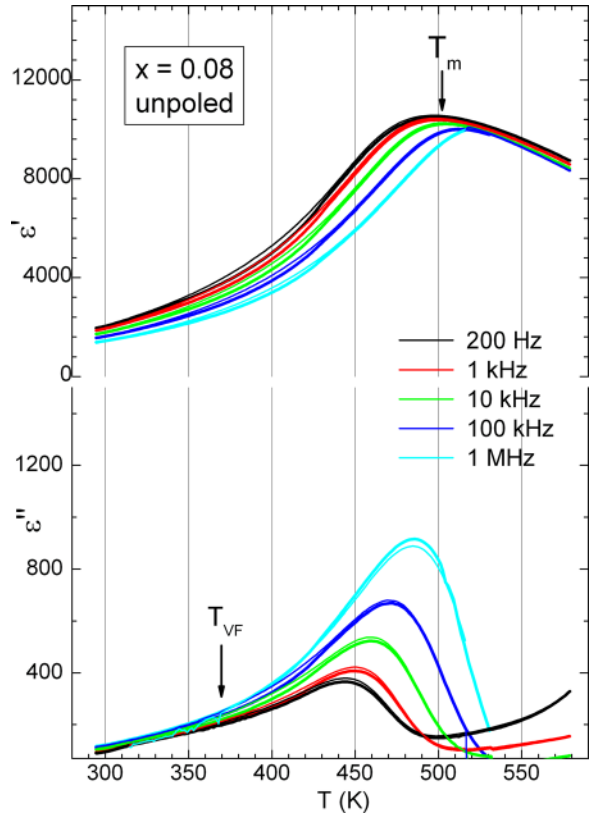

FIG. 9. Real ε' and imaginary ε'' permittivities versus temperature, measured on an unpoled x = 0.08 sample at five frequencies in the range 200 Hz–1 MHz, both on heating and cooling.

broad aspect of this peak in Fig. 1) but not enough to establish a ferroelectric state. A similar effect concerning tetragonal distortion in x = 0.08 unpoled samples was observed also in Ref. 13.

With this picture in mind, the dielectric spectra of the MPB compositions in Figures 7 and 9 can be understood. The relaxor behavior revealed in these plots is due to the dielectric response of the system of interacting PNRs and their thermal evolution.[22,23] At high temperatures, the PNRs are mobile and their behavior is ergodic. On cooling, their dynamics becomes very slow, and at the freezing temperature, the PNRs are frozen in a non-ergodic (glassy) state. A broad peak is measured in the dielectric response, and the average symmetry of the glassy state is cubic.

Relaxor dynamics is characterized by a broad distribution of relaxation times and the divergence of the longest relaxation time according to VF law $\tau = \tau_0 e^{\frac{E_a}{k(T-T_{VF})}}$ or, in terms of frequency,

$$\omega = \omega_0 e^{-\frac{E_a}{k(T-T_{VF})}}. \quad (1)$$

E_a is the activation energy for the polar cluster reorientation, T_{VF} is the Vogel-Fulcher or freezing temperature, and ω_0 is the attempt frequency. The VF law has been experimentally observed, besides relaxors, in many other complex systems like magnetic spin glasses, electric dipolar glasses, polymers, and a model has been proposed for relaxor ferroelectrics by introducing a mesoscopic mechanism for the growth of PNRs with decreasing temperature.[25]

The usual way to extract the characteristic quantities from the dielectric permittivity $\varepsilon(\omega,T)$ is to obtain the dielectric maximum temperature T_m at each measurement frequency ω and to make a fitting of $\omega(T_m)$ data with Eq. (1). The obtained parameters for three of our compositions, x = 0.04, x = 0.06 and 0.08 samples are listed in Table I, together with results from literature regarding a classical relaxor, $Pb(Mg_{1/3}Nb_{2/3})O_3$ (PMN)[26] and $Pb(Sc_{1/2}Nb_{1/2})O_3$ (PSN).[27] (The x = 0.04 sample and PSN will be discussed in Sec. III B 2). It can be observed that the activation energy and attempt frequency values are in the order of magnitude of those found in PMN.

In Fig. 11, the experimental data are represented as $1/(T_m-T_{VF})$ versus ω for each sample. The continuous lines are the results of fitting with VF law. The experimentally determined T_{VF} temperatures for each composition are marked by arrows in Figures 7 and 9.

The nonergodic phase of a relaxor ferroelectric can be transformed into a ferroelectric state by poling with a dc electric field (higher than a certain threshold value E_c, specific for each composition), but upon heating the ferroelectric state transforms back into the nonergodic state at the temperature T_d.[22,23] This is what is observed in Figures 8 and 10 for x = 0.06 and 0.08 poled samples. The ferroelectric state below T_d shows very small dispersion, unlike the relaxor state above T_d. A structural transformation accompanies also the poling process, as previously discussed. The

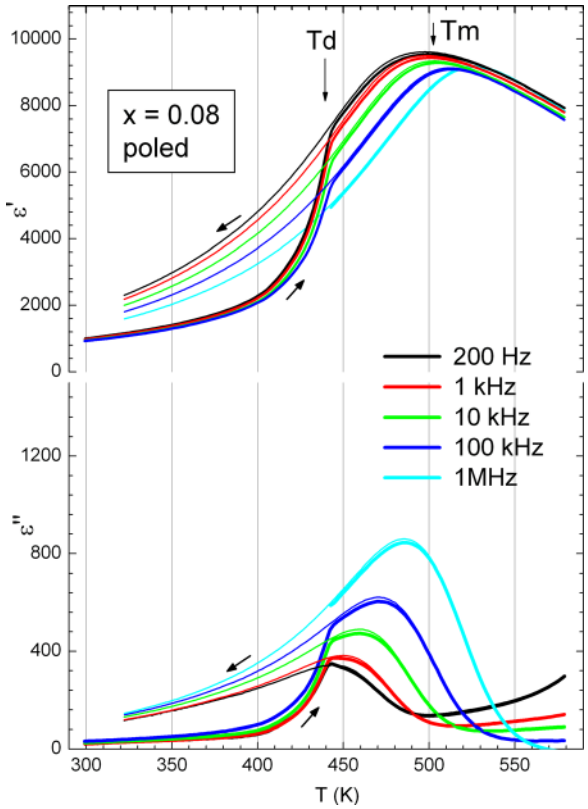

FIG. 10. The same as in Fig. 9, but on a poled x = 0.08 sample. The short arrows near the curves mark the heating and cooling.

x = 0.06 sample transforms from almost cubic to a state of coexistence of T and R phases. Thus, the structural field-induced phase transition is a consequence of a microdomain-to-macrodomain transformation, which occurs when a ferroelectric relaxor state, or a system of interacting PNRs, is transformed in a ferroelectric state by poling.

Depending on the sample state (unpoled or poled), different transformation stages are expected during heating, starting from the low temperature state formed by P4bm PNRs (unpoled state), or R3c and P4mm normal ferroelectric domains (poled state). In the unpoled state, the PNRs are visible only in the SAED patterns. In the poled state, the macroscopic phases give rise to splittings of the (111) and (200) pseudocubic peaks in the XRD patterns. This is visible also in the dielectric measurements, which show increased dispersion in the low temperature range due to the PNRs system in the unpoled sample (Fig. 7) but very small dispersion in the normal domain state of the poled sample (Fig. 8, heating curves). On increasing temperature, in the unpoled sample, there is a thermal evolution of the interacting PNRs system, reflected in the broad maximum of dielectric permittivity (Fig. 7). The inverse process occurs on cooling. In the poled sample (Fig. 8, heating curves), at T_d, the R3c +P4mm polar domains break into PNRs and the ferroelectric induced state returns relaxor above T_d. On increasing temperature, the PNRs system evolves further, giving rise to the broad maximum at T_m. On cooling, the ferroelectric extended phase is not reached due to the strength of the local random fields, and the system remains in the relaxor phase.

A similar evolution is displayed also by x = 0.08 sample, with the difference that the ground state of the poled sample is formed by the macroscopic induced P4mm ferroelectric domains which transform in P4bm nanodomains at Td.

TABLE I. Activation energy E_a, attempt frequency, and freezing temperature obtained from fitting with Vogel-Fulcher law.

Sample	Ea (meV)	ω_0 (Hz)	T_{VF} (K)
NBT-BT, x = 0.04	29	5.9×10^{10}	408.6
NBT-BT, x = 0.06	120.5	3.8×10^{12}	356.7
NBT-BT, x = 0.08	161	6.6×10^{13}	369.3
PMN	78.5	10^{12}	217
PSN	18	3.5×10^{11}	368

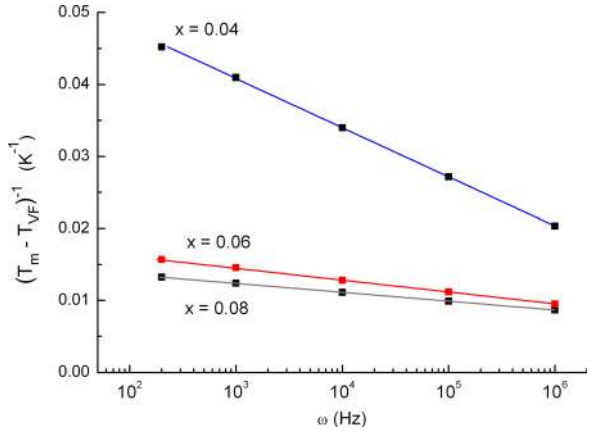

FIG. 11. Experimental data $\omega(T_m)$ represented as $1/(T_m-T_{VF})$ versus ω for different compositions. The continuous lines are the results of fitting with Vogel-Fulcher law.

2. Rhombohedral compositions

Fig. 12 shows the dielectric curves for x = 0.04 samples measured during heating and cooling, on poled and unpoled specimens at five different frequencies between 200 Hz and 1 MHz. T_d marks the depolarization temperature on heating and T_c the ferroelectric transition on cooling. T_d is higher on poled than on unpoled samples. T_m marks the temperatures of the dielectric permittivity maxima, which shift with frequency increasing towards higher temperatures, although this shift is smaller than for MPB compositions.

It has been observed in XRD spectra (Figures 1 and 2) that there is not a qualitative difference between poled and unpoled samples for rhombohedral compositions. This is reflected also in the dielectric spectra shown in Fig. 12. The sample is in the ferroelectric state below T_d in both unpoled and poled states, and only the value of T_d is displaced towards higher temperature in the case of poled sample. However, we must note the higher values shown by dielectric permittivity dispersion and loss in the ferroelectric state by the unpoled sample. This aspect is common to all measured rhombohedral compositions. It has been shown by detailed TEM and PFM studies that the ground state of these compositions is not pure ferroelectric R3c state, but is an inhomogeneous state, where R3c domains are mixed with Pbm nanodomains of refined size and higher concentration on

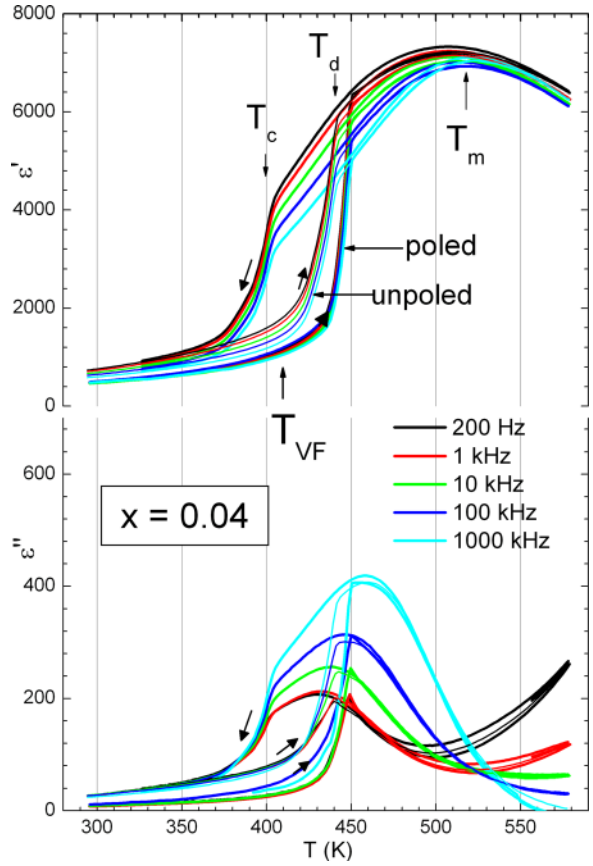

FIG. 12. Dielectric curves for $x = 0.04$ samples measured during heating and cooling, on poled and unpoled specimens at five different frequencies between 200 Hz and 1 MHz. The short arrows near the curves mark the heating and cooling.

increasing x content toward MPB.[10,15] Thus, the presence of P4bm nanodomains in the R3c phase could be the origin of the dispersion in the ferroelectric state of the unpoled samples. During poling, the P4bm nanodomain phase transforms into the macroscopic ferroelectric R3c phase.[10] We presume that this transformation is responsible for both T_d increasing and absence of dispersion in the ferroelectric state of poled samples.

Let us look now at the dielectric behavior above T_d.

It has been shown by *in situ* TEM[17] that the volume occupied by R3c complex domains on heating above T_d shrinks gradually in favour of a phase formed by nanodomains with P4bm symmetry (as confirmed by SAED diffraction patterns showing $\frac{1}{2}$(ooe) spots). Moreover, a correlated electron diffraction and *in situ* neutron diffraction study on $x = 0.04$ samples[19] showed the disappearance of the reflections $\frac{1}{2}$(ooo) typical of the rhombohedral R3c ferroelectric phase at T_d, only the reflections typical of a pseudocubic phase being observed above this temperature. Thus, with increasing temperature, the ground state of rhombohedral compositions consisting of R3c ferroelectric domains (with a minor phase of PNRs of P4bm symmetry, but in progressive amount when x is approaching MPB value) evolves to a state formed by P4bm PNRs above T_d. The successive thermal evolution of PNRs system gives rise to the increased dispersion above T_d and to the broad dielectric peak at T_m (Fig. 12).

On cooling from $T > T_m$, the inverse process occurs. Increasing correlations between PNRs with decreasing temperature as well as a slowing down of their motion gives rise to the broad dielectric peak at T_m. Further thermal evolution in a relaxor ferroelectric would result into freezing of the system of PNRs at T_{VF}, as in MPB compositions. However in $x = 0.04$ (and other rhombohedral compositions) due to less disorder and larger size of PNRs, strong correlations develop between them, which collapse the relaxor state in a ferroelectric state at T_c, in what is called, alternatively, a relaxor-to-ferroelectric (RF) or microdomain-to-macrodomain transition. The differences with the MPB compositions is that in this case, the ferroelectric transition occurs without an applied electric field, and is, therefore, called spontaneous. Spontaneous RF transitions have been found in different disordered ferroelectrics, like (Pb, La)(Zr,Ti)O_3 (PLZT),[28] PSN[27] etc. It has been shown that these transitions are accompanied also by structural phase transitions. In the case of PSN, a pseudocubic-to-rhombohedral transformation occurs on cooling at T_c. This has been observed also in $x = 0.04$ NBT-BT samples by *in situ* neutron diffraction study, which showed the disappearance of the reflections $\frac{1}{2}$(ooo) typical of the rhombohedral R3c ferroelectric phase at T_d, only the reflections typical of a pseudocubic phase being observed above this temperature.[19]

In order to obtain information about the relaxor properties and the "missed" frozen state of the $x = 0.04$ NBT-BT sample, we have fitted the $\omega(T_m)$ data obtained from dielectric measurements with Vogel-Fulcher law (Eq. (1)). The experimental data are represented as $1/(T_m\text{-}T_{VF})$ versus ω in Fig. 11. The continuous line is the result of fitting with VF law. The obtained parameters are listed in Table I, together with those corresponding to PSN.[27]

The obtained freezing temperature $T_{VF} = 408.6$ K is marked with an arrow on the dielectric curves in Fig. 12. Remarkably, it shows that the freezing, would the slowing down of PNRs motion continue as in a true relaxor, could occur at a temperature in between T_d and T_c, within the thermal hysteresis range of the ferroelectric transition, as observed also in PSN.[27]

Fig. 13 shows the dielectric curves for rhombohedral compositions $x = 0.02$, 0.03, 0.04, and 0.05 measured on heating and cooling on unpoled samples, displayed only at $\omega/2\pi = 10$ kHz, for clarity. The frequency dispersion of the dielectric maximum at T_m was observed for all compositions, although of decreased extension for lower x, but we never observed the secondary maximum (hump) between T_d and T_m as found by other investigators. However, similar behavior as in our samples was reported also by other authors.[19,29]

The increasing of the frequency dispersion and the broadening of the dielectric maximum at T_m with x are accompanied by the decreasing of the ferroelectric transition temperatures, T_d and T_c, and the increasing of $T_d\text{-}T_c$ difference.

In order to render more evident the relationship between the relaxor properties and the thermal hysteresis of the ferroelectric transition, we have plotted in Fig. 14 the dispersion at T_m, $\Delta T_m = T_m(\omega_5)\text{-}T_m(\omega_1)$, ω_1 and ω_5 being the

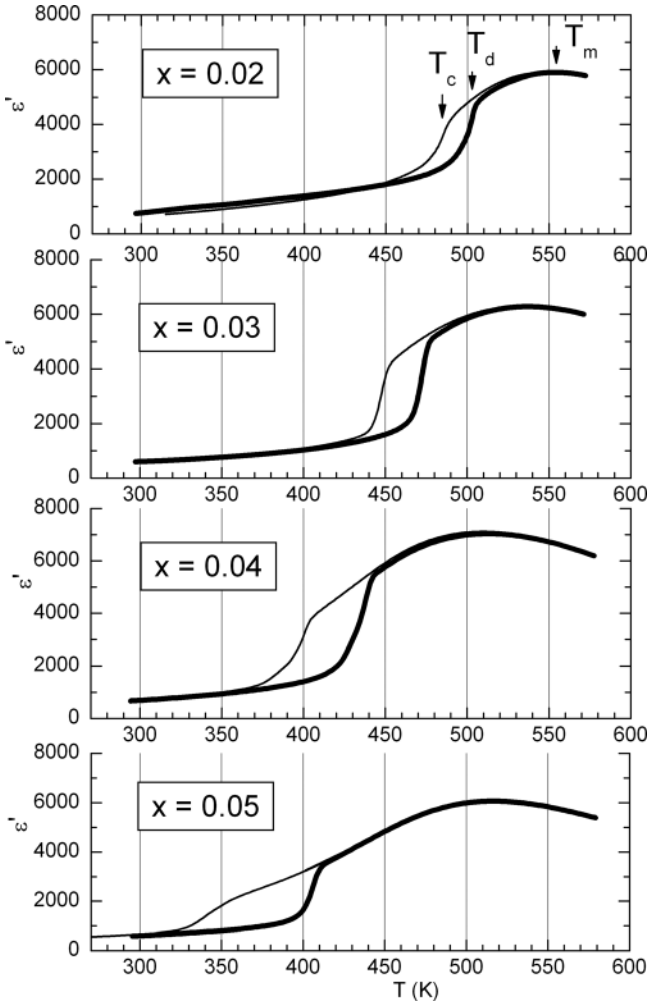

FIG. 13. Dielectric curves for rhombohedral compositions x = 0.02, 0.03, 0.04, and 0.05 measured on heating and cooling on unpoled samples, at $\omega/2\pi = 10$ kHz.

frequency limits of the measurement range, and the thermal hysteresis $\Delta T_d = T_d\text{-}T_c$, versus x. It can be observed that both increase with x content. ΔT_m represents the strength of the relaxor character and ΔT_d is related to the nucleation of the relaxor/ferroelectric phase during heating/cooling. They are both conditioned by the degree of correlations between ferroelectric clusters. However, more investigations are necessary to better understand their dependence on composition.

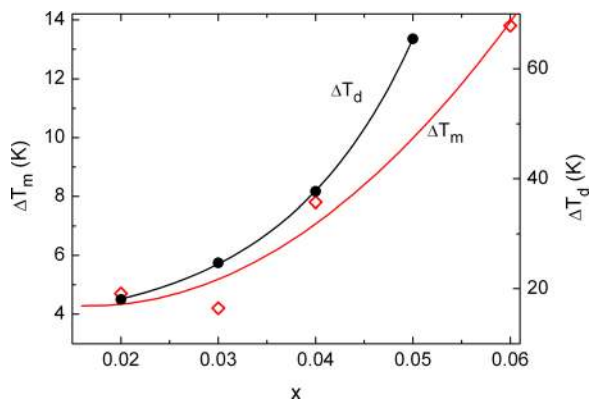

FIG. 14. The dispersion at T_m, $\Delta T_m = T_m(\omega_5)\text{-}T_m(\omega_1)$, ω_1 and ω_5 being the frequency limits of the measurement range, and the thermal hysteresis of T_d, $\Delta T_d = T_d\text{-}T_c$, versus x.

IV. CONCLUSIONS

We have investigated the relaxor properties and the ferroelectric phase transitions of lead-free $(Na_{1/2}Bi_{1/2})_{1-x}Ba_xTiO_3$ ceramics, with $0 \leq x \leq 0.08$. Electric field-induced and spontaneous relaxor-ferroelectric phase transitions have been found in MPB and, respectively, in rhombohedral compositions. The frequency dispersion of the dielectric peak at T_m has been analysed with Vogel-Fulcher law. The activation energy and attempt frequency for the MPB compositions are similar to those typical for classical relaxors like $Pb(Mg_{1/3}Nb_{2/3})O_3$, while for rhombohedral compositions, they are of the order of magnitude of those found in relaxor ferroelectrics with spontaneous relaxor-ferroelectric phase transitions, like PSN. The Vogel-Fulcher temperature for rhombohedral compositions lies within the hysteresis range of ferroelectric transition. It has been found also that both the relaxor dispersion at T_m and the hysteresis of the ferroelectric transition increase with x content.

ACKNOWLEDGMENTS

The authors thank C. Capiani for the skilful preparation of the samples, and P. M. Latino and F. Corvasce for technical assistance.

[1]T. Takenaka, K. Maruyama, and K. Sakata, Jpn. J. Appl. Phys., Part 1 **30**, 2236 (1991).
[2]Y. Hosono, K. Harada, and Y. Yamashita, Jpn. J. Appl. Phys., Part 1 **40**, 5722 (2001).
[3]N. Yasuda, S. Hashimoto, H. Ohwa, O. Sakurada, K. Fujita, Y. Yamashita, M. Iwata, and Y. Ishibashi, Jpn. J. Appl. Phys., Part 1 **48**, 09KC06 (2009).
[4]M. Chen, Q. Xu, B. H. Kim, B. K. Ahn, J. H. Ko, W. J. Kang, and O. J. Nam, J. Eur. Ceram. Soc. **28**, 843 (2008).
[5]K. Hiruma, K. Yoshii, H. Nagata, and T. Takenaka, Ferroelectrics **346**, 114 (2007).
[6]B. W. van Eerd, D. Damjanovic, N. Klein, N. Setter, and J. Trodahl, Phys. Rev. B **82**, 104112 (2010).
[7]C. Ma, X. Tan, E. Dul'kin, and M. Roth, J. Appl. Phys. **108**, 104105 (2010).
[8]F. Cordero, F. Craciun, F. Trequattrini, E. Mercadelli, and C. Galassi, Phys. Rev. B **81**, 144124 (2010).
[9]W. Jo, J. E. Daniels, J. L. Jones, X. Tan, P. A. Thomas, D. Damjanovic, and J. Rödel, J. Appl. Phys. **109**, 014110 (2011).
[10]C. Ma, H. Guo, S. P. Beckman, and X. Tan, Phys. Rev. Lett. **109**, 107602 (2012).
[11]K. Roleder, J. Franke, A. M. Glazer, P. A. Thomas, S. Miga, and J. Suchanicz, J. Phys.: Condens. Matter **14**, 5399 (2002).
[12]G. O. Jones and P. A. Thomas, Acta Crystallogr. B **58**, 168 (2002).
[13]G. Picht, J. Töpfer, and E. Hennig, J. Eur. Ceram. Soc. **30**, 3445 (2010).
[14]J. Yao, L. Yan, W. Ge, L. Luo, J. Li, D. Viehland, Q. Zhang, and H. Luo, Phys. Rev. B **83**, 054107 (2011).
[15]J. Yao, N. Monsegue, M. Murayama, W. Leng, W. T. Reynolds, Q. Zhang, H. Luo, J. Li, W. Ge, and D. Viehland, Appl. Phys. Lett. **100**, 012901 (2012).
[16]J. Yao, W. Ge, Y. Yang, L. Luo, J. Li, D. Viehland, S. Bhattacharyya, Q. Zhang, and H. Luo, J. Appl. Phys. **108**, 064114 (2010).
[17]C. Ma and X. Tan, J. Am. Ceram. Soc. **94**, 4040 (2011).
[18]R. Ranjan and A. Dviwedi, Solid State Commun. **135**, 394 (2005).
[19]J. Wang, Y. Liu, R. L. Withers, A. Studer, Q. Li, L. Norén, and Y. Guo, J. Appl. Phys. **110**, 084114 (2011).
[20]E. Sapper, S. Schaab, W. Jo, T. Granzow, and J. Rödel, J. Appl. Phys. **111**, 014105 (2012).
[21]A. M. Glazer, Acta Crystallogr. B **28**, 3384 (1972).

[22]G. A. Samara, *Ferroelectricity Revisited—Advances in Materials and Physics, Solid State Physics*, Vol. 56, edited by H. Ehrenreich and F. Spaepen (Academic, San Diego, 2001), pp. 239–458.
[23]A. A. Bokov and Z.-G. Ye, J. Mater. Sci. **41**, 31 (2006).
[24]W. Jo, S. Schaab, E. Sapper, L. A. Schmitt, H.-J. Kleebe, A. J. Bell, and J. Rödel, J. Appl. Phys. **110**, 074106 (2011).
[25]R. Pirc and R. Blinc, Phys. Rev. B **76**, 020101(R) (2007).
[26]D. Viehland, L. E. Cross, and M. Wuttig, Ferroelectrics **120**, 71 (1991).
[27]F. Chu, I. M. Reaney, and N. Setter, J. Appl. Phys. **77**, 1671 (1995).
[28]X. Dai, A. DiGiovanni, and D. Viehland, J. Appl. Phys. **74**, 3399 (1993).
[29]J. Suchanicz, J. Kusz, H. Böhm, and G. Stopa, J. Mater. Sci. **42**, 7827 (2007).